Inorg. Chem. **2008**, *47*, 6659−6673

Medium and Interfacial Effects in the Multistep Reduction of Binuclear Complexes with Robson-Type Ligand

Renat R. Nazmutdinov,*,† Nataliya V. Roznyatovskaya,*,‡ Dmitrii V. Glukhov,† Ibragim Manyurov,† Vladimir M. Mazin,‡ Galina A. Tsirlina,‡ and Michael Probst§

Kazan State Technological University, K. Marx Str., 68 420015 Kazan, Russian Federation, Department of Electrochemistry, Faculty of Chemistry, Moscow State University, Leninskie Gory1- str.3, Moscow 119992, Russian Federation, and Institute of Ions Physics and Applied Physics, University of Innsbruck, A-6020 Innsbruck, Austria

Received December 30, 2007

We present a combined experimental and computational approach to the modeling and prediction of reactivity in multistep processes of heterogeneous electron transfer. The approach is illustrated by the study of a Robson-type binuclear complex (−Cu(II)−Cu(II)−) undergoing four-electron reduction in aqueous media and water-acetonitrile mixtures. The observed effects of solvent, pH, buffer capacity, and supporting electrolyte are discussed in the framework of a general reaction scheme involving two main routes; one of them includes protonation of intermediate species. The main three problems are addressed on the basis of modern charge transfer theory: (1) the effect of the nature of reactant and intermediate species (protonated/deprotonated, bare or associated with supporting anion/solvent molecule) on the standard redox potential, the electronic transmission coefficient, and the intramolecular reorganization; (2) possible effect of protonation on the shape of the reaction free energy surfaces which are built using the Anderson Hamiltonian; (3) electron transfer across an adsorbed chloride anion. Quantum chemical calculations were performed at the density functional theory level.

I. Introduction

Quantum chemical modeling of heterogeneous charge transfer provides an approach to predict the kinetic behavior of "simple" electrode reactions,[1] including the dependence of the reaction rate (current density) on electrode potential, solution composition, and electrode nature. To apply similar approaches straightforwardly to multistep reactions, it is necessary to model a number of electrochemical and chemical steps. Moreover, recognition of real active species (protonated or deprotonated form, separate ion or ionic associate, etc.) is frequently a challenge even for a single step reaction and also for complex processes, and it is necessary to understand the real composition of many species including intermediates. We believe that often time-consuming modeling can be avoided if the analysis of experimental facts is combined with a limited number of computational efforts. Even qualitative conclusions made on the basis of such an analysis facilitates and reveals a general reaction scheme.

Our approach, discussed in detail below, is applied to the multielectron reduction of $[Cu_2L]Cl_2$ where L is the product of the [2 + 2] condensation of 2,6-diformyl-4-*t*-butylphenol and 1,3-diaminopropane, Figure 1.

Figure 1 presents the most general possible reaction pathway including 4-electron reduction of two central ions and the subsequent ligand reduction.[2] The left and right arrows in the first step relate to proton reduction and proton-assisted reduction, respectively. This process is a representative example of medium-dependent multistep electrode processes as follows from the significant difference in the experimentally observed redox behavior in nonaqueous[3] and aqueous[4] media: two well-separated single electron waves appear in nonaqueous solvents, whereas one 4-electron wave

* To whom correspondence should be addressed. E-mail: nazmutdi@kstu.ru (R.R.N.), natasha@elch.chem.msu.ru (N.V.R.). Fax: +78432365768.
† Kazan State Technological University.
‡ Moscow State University.
§ University of Innsbruck.

(1) (a) Nazmutdinov, R. R.; Tsirlina, G. A.; Petrii, O. A.; Kharkats, Yu. I.; Kuznetsov, A. M. *Electrochim. Acta* **2000**, *45* (1), 3521–3536. (b) Nazmutdinov, R. R. *Russ. J. Electrochem.* **2002**, *38* (2), 111–122.

(2) We do not consider an alternative scheme with initial ligand reduction because we deal with transition metal complexes. The simultaneous reduction of the central ions and the ligand (for example, $E_1 = E_2 = . . E_n$) can be treated as a limiting case of the scheme in Figure 1.

10.1021/ic702511w CCC: $40.75
Published on Web 06/27/2008

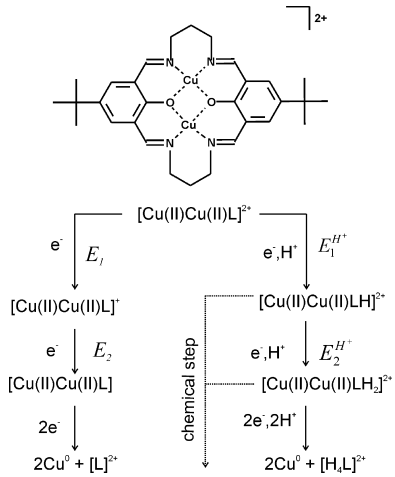

Figure 1. Schematic representation of $[Cu_2L]Cl_2$ reduction pathways.The potentials of redox transitions are denoted by *E*.

is found in buffered aqueous solutions. A similar behavior is known for other types of complex compounds, including porphyrines and phtalocyanines.[5]

At least two independent general hypotheses can be formulated to explain the solvent-dependent behavior. Hypothesis (I) rests on the important role of protonation affecting the redox equilibria with participation of intermediate species and/or the kinetics of some steps, that is, realization of the left pathway branch (Figure 1) in aprotic medium and of the right branch (Figure 1) in protic medium.[8] Hypothesis (II) presumes a solvent-dependent structure of the reacting species, that is, solvent molecules (hypothesis IIa) or supporting electrolyte anions in a certain solvent (hypothesis IIb) bound to the unsaturated central ion and, finally, the solvent-dependent adsorption behavior (hypothesis IIc). Of course, some "mixed" versions may be also considered.

The experiments presented in this paper are aimed first of all to find the most influential factors related to solution composition. The results of this diagnostic are used for formulating the computational tasks which should facilitate whether to confirm or to reject certain hypotheses.

An important (and also rather representative) complication follows from the preparation of the solid reactants under study. All reactants of this type (complexes with L or related substituted ligands) are available mostly as crystalline hydrates. This means that in any solvent (including aprotic [2,6,7]) the water, counterion, and reactant concentrations are comparable. It is difficult, therefore, to separate any other effects from the effect of chloride bonding, if the latter is significant. This is why special attention is put on a computational study of various adducts. Taking into account the unavoidable presence of water even in "nonaqueous" media in the absence of buffer (typical conditions[3]), we also pay some attention on a comparison of aqueous buffered and unbuffered solutions.

This paper is organized as follows. In Section II we present experimental details. Section III collects experimental observations on the effects of protons, supporting anions, and acetonitrile (AN) on the shape and height of $[Cu_2L]Cl_2$ reduction wave. These data constitute a platform for formulating the most challenging points for a computational study in the framework of quantum chemical methods and modern theories of charge transfer. The results of model calculations of key kinetic parameters are discussed in detail in the most broadened section 3. Some concluding remarks are contained in section 4.

II. Experimental Techniques

All polarographic measurements in direct current (DC) mode were performed at a dropping mercury electrode (flow rate of 0.84 mg s^{-1}; open circuit drop lifetime of 7.8 s) in a three-electrode cell. A reference electrode was saturated calomel electrode (SCE). All solutions were deaerated with hydrogen before each measurement. Currents are presented with subtraction of the background. Other details can be found in ref 4a. Cyclic voltammograms in organic and mixed (organic-water) solvents were measured in a specially designed cell (for the measurement details and protocol see Supporting Information). Platinum and silver wires were used as working and quasi-reference electrodes, respectively. The reference electrode was calibrated via ferrocene/ferrocenium redox pair at the end of each measurement. It is necessary to note that the solubility of $[Cu_2L]Cl_2$ in a water-free AN background solution turned out to be rather poor, and the added amount of the substance calculated for 1 mM concentration did not dissolve completely, so that in the real concentration was 0.1−0.5 mM. Though, after

(3) (a) Gagne, R. R.; Koval, C. A.; Smith, T. J.; Cimolino, M. C. *J. Am. Chem. Soc.* **1979**, *101*, 4571–4580. (b) Lacroix, P.; Kahn, O.; Theobald, F.; Leroy, J.; Wakselman, C. *Inorg. Chim. Acta* **1988**, *142*, 129–134. (c) Long, R. C.; Hendrickson, D. N. *J. Am. Chem. Soc.* **1983**, *103*, 1513–1521. (d) Mandal, S. K.; Adhikary, B.; Nag, K. *J. Chem. Soc., Dalton. Trans.* **1986**, 1175–1186. (e) Nanda, K. K.; Addison, A. W.; Paterson, N.; Sinn, E.; Thompson, L. K.; Sakaguchi, U. *Inorg. Chem.* **1998**, *37*, 1028–1036.

(4) (a) Roznyatovskaya, N. V.; Tsirlina, G. A.; Roznyatovskii, V. V.; Reshetova, M. D.; Yustinyuk, Yu. A. *Russ. J. Electrochem.* **2004**, *40* (9), 955–962. (b) Roznyatovskaya, N. V.; Tsirlina, G. A.; Roznyatovskii, V. V.; Mitiaev, A. S.; Smurnyy, Y. D. *Mendeleev Commun.* **2005**, *15* (3), 93–95. (c) Roznyatovskaya, N. V.; Vassiliev, S. Yu.; Yusipovich, A. I.; Tsirlina, G. A.; Roznyatovskii, V. V. *J. Solid State Electrochem.* **2005**, *9* (8), 581–589.

(5) (a) Lever, A. B. P., Milaeva, E. V., Speier, G. The Redox Chemistry of Metallophthalocyanines in Solution. In *Phthalocyanines: properties and application*; Leznoff, C. C., Lever, A. B. P., Eds.; Wiley-VCH Verlag GmbH: Germany, 1993; Vol. *3*, pp 1−303. (b) *The Porphyrin Handbook*; Kadish, K. M., Smith, K. M., Guilard, R., Eds.; Academic Press: San Diego, CA, 2000; Vol. *9*, Chapter 59, pp 1−212.

(6) Pilkington, N. H.; Robson, R. *Aust. J. Chem.* **1970**, *23*, 2225–2236.

(7) (a) Gagne, R. R.; Spiro, C. L.; Smith, T. J.; Hamann, C. A.; Thies, W. R.; Shiemke, A. K. *J. Am. Chem. Soc.* **1981**, *103*, 4073–4081. (b) Gagne, R. R.; Henling, L. M.; Kistenmacher, T. J. *Inorg. Chem.* **1980**, *19*, 1226–1231. (c) Long, R. C.; Hendrickson, D. N. *J. Am. Chem. Soc.* **1983**, *105*, 1513–1521. (d) Nanda, K. K.; Addison, A. W.; Paterson, N.; Sinn, E.; Thompson, L. K.; Sakaguchi, U. *Inorg. Chem.* **1998**, *37*, 1028–1036. (e) Mandal, S. K.; Nag, K. *Inorg. Chem.* **1983**, *22*, 2567–2572. (f) Mandal, S. K.; Nag, K. *J. Chem. Soc., Dalton Trans.* **1983**, 2429–2434. (g) Mandal, S. K.; Nag, K. *J. Chem. Soc., Dalton Trans.* **1984**, 2141–2149. (h) Addison, A. W. *Inorg. Nucl. Chem. Lett.* **1976**, *12*, 899–903. (i) Mandal, S. K.; Thompson, L. K.; Charland, J.-P.; Gabe, E. J. *Can. J. Chem.* **1987**, *65*, 2815–2853. (j) Mandal, S. K.; Thompson, L. K.; Nag, K.; Charland, J.-P. *Inorg. Chem.* **1987**, *26*, 1391–1395. (k) Mandal, S. K.; Thompson, L. K.; Newlands, M. J.; Gabe, E. J. *Inorg. Chem.* **1989**, *28*, 3707–3713. (l) Gagne, R. R.; Koval, C. A.; Smith, T. J. *J. Am. Chem. Soc.* **1977**, *99*, 8367–8368. (m) Okawa, H.; Tadokoro, M.; Aratake, Y.; Ohba, M.; Shindo, K.; Mitsumi, M.; Koikawa, M.; Tomono, M.; Fenton, D. E. *J. Chem. Soc., Dalton Trans.* **1993**, 253–258. (n) Karunakaran, S.; Kandaswamy, M. *J. Chem. Soc., Dalton Trans.* **1994**, 1595–1598. (o) Tandon, S. S.; Thompson, L. K.; Bridson, J. N.; McKee, V.; Downard, A. J. *Inorg. Chem.* **1992**, *31*, 4635–4642. (p) Chatterjee, K. K.; Farrier, N.; Douglas, B. E. *J. Am. Chem. Soc.* **1962**, *85*, 2919–2922.

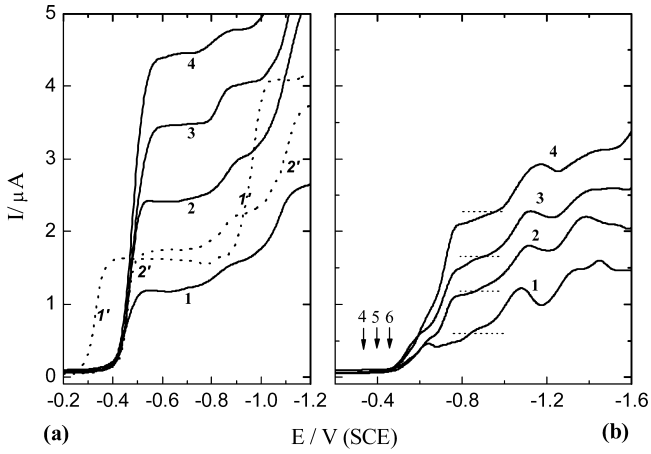

Figure 2. DC polarograms of solutions: (solid curves) x mM of $[Cu_2L]Cl_2$ (x: (1) 0.2, (2) 0.4, (3) 0.6, (4) 0.8) + (a) 0.1 M acetate buffer (pH 6), (b) 0.1 M AcONa (pH 8); (dashed curves) 0.2 mM of $[Cu_2L]Cl_2$ + 0.1 M acetate buffer; pH: (1′) 4.0, (2′) 6.0. The horizontal marks correspond to the two-electrons reduction of $[Cu_2L]Cl_2$ (see text).

addition of water the solubility (and thus the concentration) increased. This is the reason why we consider the data for mixed solvents only at a qualitative level.

Chemicals. $CH_3COONa \cdot 3H_2O$ (AcONa), glacial acetic acid (pure per analysis, Merck), KCl, and NaF (pure per analysis, Khimmed) were used for preparation of a supporting solution. KCl and NaF were purified by triple recrystallization. Demineralized water used to prepare solutions was additionally purified by passing it through a Millipore-Milli-Q system, the final resistivity being at least 18 $M\Omega \cdot cm^{-1}$. Acetonitrile and dichloromethane were Sigma-Aldrich reagents (HPLC grade 99.9%). Tetrabutylammonium hexafluorophosphate (puriss. electrochemical grade ≥99.0%, Fluka) was used as supporting electrolyte. $[Cu_2L]Cl_2 \cdot H_2O$ was prepared and characterized following a literature method.[6] Analytical data for $[Cu_2L]Cl_2 \cdot H_2O$ were reported previously in ref 4c.

III. Experimental Results

(i) Effect of pH and Buffer Capacity: Preliminary Assumptions about the Role of Protonation. We start with a comparison of a typical series of polarograms registered in acetate buffer solution of $[Cu_2L]Cl_2$. Figure 2a is compared to a similar series in sodium acetate solution, pH ∼ 8, in Figure 2b. In the buffered solution, the first wave describes the four-electron pH-dependent reduction of $[Cu_2L]Cl_2$ with the formation of metallic copper and a free ligand which hydrolyzes in water.[4a]

A noticeable splitting of the above mentioned wave is observed in the absence of buffer with the appearance of at least three (sometimes four) smaller waves. The shift of the first reduction wave is in general agreement with the pH dependence in buffered media observed earlier (64 ± 3 mV/pH)[4a] (arrows in Figure 2b indicate the half-wave potentials at pH 4, 5, and 6). This behavior of the first wave corresponds to the first step in the right branch of the reaction pathway in Figure 1. However, in contrast to the reaction in the buffered medium, the first step induces some increase of local pH because the resumption of protons is limited by their transport from the solution bulk. The next two waves (which relate already to a higher local pH) are observed at the potentials more negative than −0.7 V. For the waves corresponding to transfer of subsequent electrons, the plateaus of limiting diffusion current are poorly recognized. The limiting current at −0.6 V is proportional to the $[Cu_2L]Cl_2$ concentration, when no dependence of current on $[Cu_2L]Cl_2$ concentration higher than 0.4 mM is observed for subsequent polarographic waves.

A rough estimate of the local pH change can be performed as follows, [9]

$$c_{H^+} = c_0 \cdot \sqrt{D_0/D_{H^+}} \quad (1)$$

where c_{H^+} and D_{H^+} are the local concentration and diffusion coefficient of the proton, respectively; c_0 and D_0 are the same parameters of the redox active species.

A value of 3.6×10^{-6} cm s^{-1} was found earlier for D_0;[4a] hence, the D_0/D_{H^+} ratio is 10^{-2} in magnitude. This means that for mM concentrations (c_0) at pH exceeding 4 (in nonbuffered solutions) the increase of pH is no longer compensated.

The third and possible subsequent waves exhibit broad current minima, which resemble similar polarograms measured after preparative electrolysis in ref 4a, that is, in the presence of free hydrolyzed ligand. This similarity makes it possible to assume a fast destruction of the reduction products (most probably induced from the local pH increase[9]). In other words, at higher local pH the product of two-electron or deeper $[Cu_2L]Cl_2$ reduction can undergo fast decomposition with formation of free ligand and/or its fragments that can be formed because of hydrolysis of partially reduced $[Cu_2L]Cl_2$.

Therefore, the wave with the onset at −0.8 V (demonstrating weak dependence on the reactant concentration) may be treated as an adsorption prewave describing the reduction of ligand or its destruction products. We can argue that a complex behavior of polarograms in nonbuffered solutions prevents further analysis of the third and fourth reduction steps.

No further wave splitting occurs after addition of NaOH to the solution of $[Cu_2L]Cl_2$ in acetate supporting electrolyte (curves 2, 3 in Figure 3). The height of the first wave is equal in height to the sum of the first and second wave heights in acetate solution of pH 8 (curve 1 in Figure 3). The effects of local pH in alkaline solution are less noticeable; therefore, the second single electron reduction is not accompanied most likely with protonation (see the left branch in Figure 1). An estimate using eq 1 yields about 10 as a boundary pH value for the appearance of a noticeable local alkalization.

The potential of the next wave (from −0.9 to −1.2 V) shifts toward negative values with pH. This shift amounts to about 30 mV/pH and can be interpreted as $1H^+/2$ electrons consumption.

(8) As was demonstrated in ref 4a, any of four subsequent single electron steps is accompanied with the accumulation of one additional proton; see the right branch of reaction pathway in Figure 1.

(9) (a) Tondeur, J. J.; Dombret, A.; Gierst, L. *J. Electroanal. Chem.* **1962**, *3*, 225–262. (b) Fedorovich, N. V.; Damaskin, B. B.; Botukhova, G. N.; Vorob'eva, S. A. *Russ. J. Electrochem.* **1990**, *26*, 542.

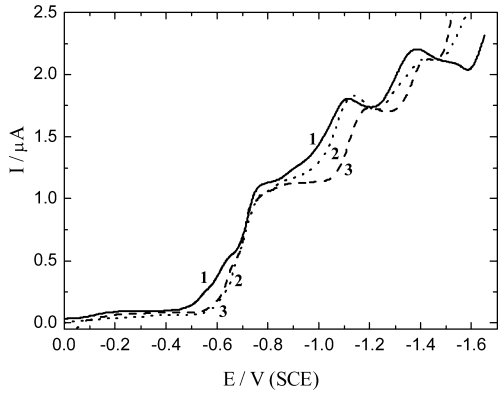

Figure 3. DC polarograms of solutions 0.4 mM $[Cu_2L]Cl_2$ + 0.1 M AcONa; pH: (1) 8.0, (2) 10.7, (3) 11.6

Because no pK_a values are available for both oxidized and reduced forms of the reactant, one cannot predict whether reduction at certain pH is accompanied with protonation or not. The left branch of the reaction scheme (Figure 1) may be ascribed to the first two waves at least for pH exceeding 10. This scheme probably works also for the second step already at lower pH of about 8. The separation of waves can result either from a higher value of $(E_1 - E_2)$ as compared with $(E_1^{H^+} - E_2^{H^+})$, or from the same difference between $(E_1^{H^+} - E_2)$ and $(E_1^{H^+} - E_2^{H^+})$. We cannot also exclude a kinetic nature of the wave separation.

(ii) Effect of Supporting Electrolyte Concentration: What Species Are More Active? To check the role of electrostatic (double layer) effects at $[Cu_2L]Cl_2$ reduction, the concentration of supporting electrolytes was varied from 0.05 to 1 M, which did not change significantly the polarograms. The possible reason is that either $[Cu_2L]Cl_2$ might be reduced in a low-charged form, or potential values on the outer Helmholtz plane are low (in the vicinity of the potential of zero charge).

Our quasiequilibrium electrocapillary measurements[10] show the shift of pzc toward more positive values, when M_2L-containing species are adsorbed. Such a behavior agrees qualitatively with the assumption of the positive charge of species. The same can be supposed from the results reported earlier for $[Cu_2L]Cl_2$ bearing 4-methyl substituent:[12] with an access of chloride or acetate anion (A^-) the binuclear species can bind these anions, as well as the solvent molecules S, forming $[Cu_2L(S)_x(A)_{2-x}]^{x+}$ ($x = 0, 1, 2$) complex species.[11] The conductivity of water solutions of Cu_2L-containing species with various counterions is reported in ref 6. It can be argued from the comparison of these data with the mobility of counterions that only the first step of $[Cu_2L]Cl_2$ dissociation is complete but certainly not the second one. However, the data in ref 6 provide some evidence in favor of a cationic nature of reactant in solution bulk.

(10) Roznyatovskaya, N. V.; Laurinavichute, V. K.; Tsirlina, G. A.; Mirsky, V. M. *J. Solid State Electrochem.* **2007**, *11*, 981–992.

(11) The aqueous solutions of $[Cu_2L]Cl_2$ with various supporting electrolytes were studied by UV-vis spectroscopy to examine possible changes in the coordination sphere of the complex species. No change of absorbance in the UV and visible regions or the wave length of the absorption peak was observed after addition of supporting electrolytes.

(12) Atkins, A. J.; Black, D.; Blake, A.J.; Marin-Becerra, A.; Parsons, S.; Ruiz-Ramirez, L.; Schröder, M. *Chem. Commun.* **1996**, 457–463.

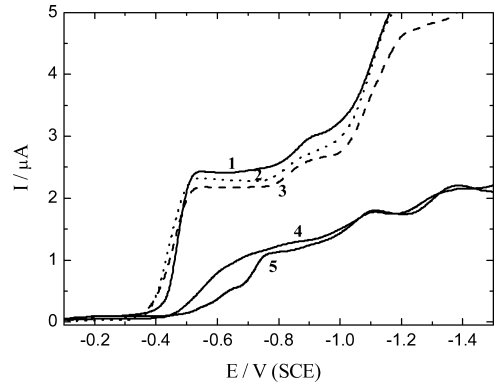

Figure 4. DC polarograms of solutions. (1) 0.4 mM of $[Cu_2L]Cl_2$ + x M acetate buffer pH 6 + y M KCl, x, y: 0.1, 0, curve 1; 0.1, 0.1, curve 2; 0.05, 0.5, curve 3; (2) 0.4 mM of $[Cu_2L]Cl_2$ + 0.1 M AcONa + 0.1 M KCl, curve 4; (3) 0.4 mM of $[Cu_2L]Cl_2$ + 0.1 M AcONa, curve 5.

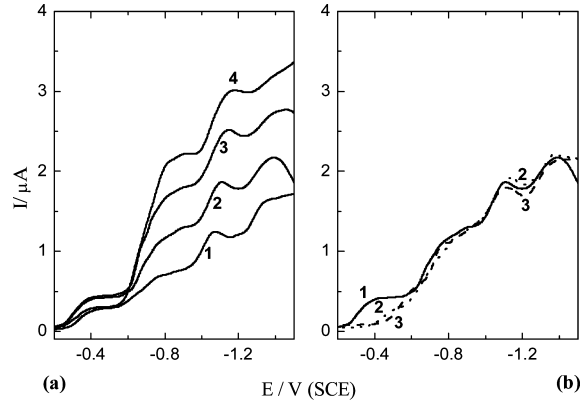

Figure 5. DC polarograms of solutions: (a) x mM $[Cu_2L]Cl_2$ + 0.1 M KCl, x: (1) 0.2, (2) 0.4, (3) 0.6, (4) 0.8. (b) 0.4 $[Cu_2L]Cl_2$ + (1) 0.1 M KCl (pH 5.5), (2) 0.1 M NaF (pH 6.0), (3) 0.1 M AcONa (pH 8.0).

Being a counterion in the salt $[Cu_2L]Cl_2$, the Cl^- anion exists in all solutions we examined. In general, the acetate and chloride anions (A), as well as solvent molecules (S), compete with each other to reside in the inner coordination shell of a $[Cu_2L(S)_x(A)_{2-x}]^{x+}$ complex. To investigate the effect of chloride bonding, a chloride salt was added to an acetate buffer solutions of $[Cu_2L]Cl_2$ (compare curves 1 and 2, 3 in Figure 4) and to an unbuffered solution (compare curves 4 and 5 in Figure 4). A slight (albeit reproducible) shift of the reduction onset toward less negative potentials is observed in the both cases, which confirms the catalytic role of chloride in the reaction under study.

A splitting of the polarographic wave at $[Cu_2L]Cl_2$ reduction was found in nonbuffered chloride supporting electrolytes (Figure 5a). The initial pH value of this solution is 5.5, and it is possible to compare the polarograms with those obtained for $[Cu_2L]Cl_2$ in a buffer solution (pH 4−6). Starting from −0.6 V polarographic currents are in the same dependence on $[Cu_2L]Cl_2$ concentration as those of $[Cu_2L]Cl_2$ in acetate electrolyte (Figure 2b). In contrast to the $[Cu_2L]Cl_2$ polarograms in acetate solution (Figure 2), the reduction onset takes place, however, at a more positive potential (prewave in Figure 5a). This prewave satisfies current-concentration independence criteria for adsorption waves (curves 1−4 in Figure 5a). The presence of an adsorption prewave in the chloride electrolyte can result from a stronger

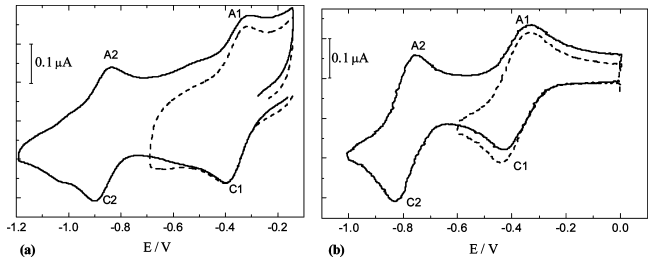

Figure 6. Cyclic voltammogram of $[Cu_2L]Cl_2$ (ca. 0.5 mM) + 0.1 M TBAP, scan rate 100 mV/s (a) in AN (dotted curve) in the potential range from −0.15 to −0.7 V, (solid curve) from −0.15 to −1.2. (b) in CH_2Cl_2 (dotted curve) in the potential range from 0 to −0.6 V, (solid curve) from 0 to −1 V. The redox couple of Fe(Cp)2 (internal reference) is observed at 0.51 V under in CH_2Cl_2.

(as compared to acetate) specific adsorption of chloride anions on a mercury electrode. The penetration of a chloride anion into the inner coordination shell of $[Cu_2L]Cl_2$, on the other hand, is also possible. In contrast to the curves in Figure 5a, polarograms in Figure 4 (measured in the mixture of acetate buffer and chloride) do not show any adsorption prewave. The problem of competitive bonding of acetate and chloride appears to be important, therefore, to interpret these data.

The $[Cu_2L]Cl_2$ reduction in fluoride supporting electrolyte starts at more negative potentials than −0.4 V (curve 2 in Figure 5b). The onset of $[Cu_2L]Cl_2$ reduction (pH of initial fluorine solution was about 6) is the same as in acetate buffer pH 6. As fluoride anions do not adsorb specifically at a mercury electrode, the absence of their effect on the reaction kinetics consolidates our interest to the possible role of adsorbed chloride ions as a "bridge" in electron transfer (ET).

(iii) Testing Nonaqueous and Mixed Systems. Most of literature data on the separation of single electron peaks in aprotic solvents[3,7] cannot be exactly related to $[Cu_2L]Cl_2$; they describe homologous complexes with alkyl-substituted ligands. The aim of our tests reported in this subsection is to examine whether the splitting of peaks is solvent-dependent in various aprotic media.

Two redox features were observed in AN and methylene chloride. The first couple of peaks at less negative potentials (Figure 6) relates to more reversible single electron processes, with square root dependence of the peak current on the scan rate at 10−500 mV s^{-1} and a negligible shift of the peak potentials with scan rate (the most detailed data of this sort were obtained for AN). Although the second couple is already less reversible, it also demonstrates a similar square root dependence of the peak currents. The difference of the first and second formal potentials was found to be 0.4−0.5 V for both two solvents. This indicates that the reason for the peak separation is hardly solvent-dependent. Literature data on the reduction of $[Cu_2L](ClO_4)_2$ with different ligand alkyl-substituent point to the region of about 0.35−0.5 V in the same solvents[3a,d,7e] as the difference of redox peak potentials. Because water is always involved in both two solutions (as a component of the solid reactant), the reason for peak separation might be a local pH increase in the reaction layer which is higher when the quantity of water is lower.

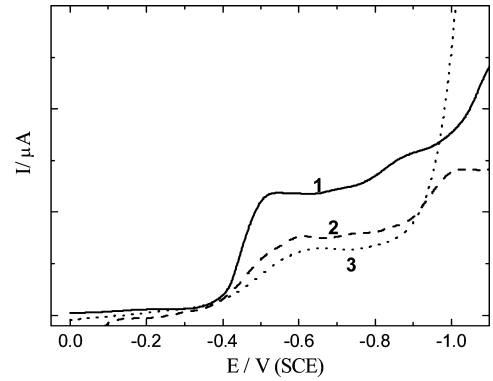

Figure 7. DC polarograms of solutions: 0.2 mM $[Cu_2L]Cl_2$ + (1) 0.1 M acetate buffer pH 6.0; 0.2 mM $[Cu_2L]Cl_2$ + 0.1 M TBAP + *x* M H_2O in AN, *x* (2) 1.1 (2% vol.), (3) 5.5 (10% vol.).

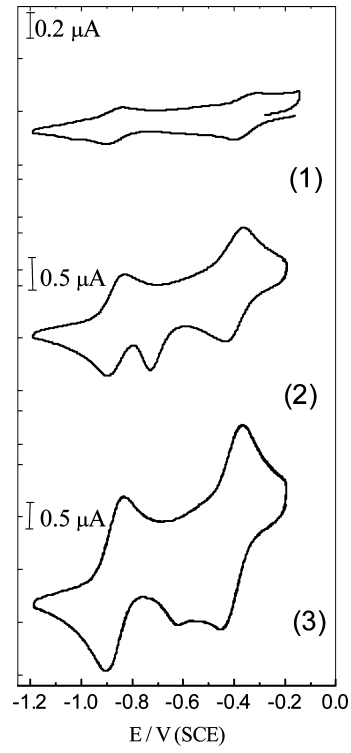

Figure 8. Cyclic voltammograms of solutions: $[Cu_2L]Cl_2$ (ca. 0.5 mM) + 0.1 M TBAP + *x* M H_2O in AN, *x* = (1) 0, (2) 0.04, (3) 0.48. Scan rate 100 mV/s.

Figures 7 and 8 display voltammetric and polarographic data for $[Cu_2L]Cl_2$ AN solutions in AN with a higher water content. A qualitative similarity with the data shown in Figure 2b makes it possible to argue that just the protons and local pH changes play a dominating role in the observed reduction difference for aqueous and "nonaqueous" media.

Because the solubility of $[Cu_2L]Cl_2$ in AN is not sufficient to get about mM solutions, the minimal amount of water was added in our experiments. The polarogram of $[Cu_2L]Cl_2$ in AN in the presence of ∼1 M of water (curve 1 in Figure 7) shows two waves in the range from −0.2 to −1.2 V. The difference in half-wave potentials of these waves is about 0.47 V. When comparing curves 1, 2, and 3 (i.e., the reduction of $[Cu_2L]Cl_2$ in aqueous buffered and water−AN media), one can see that the limiting current of the first wave is twice lower in water−AN media than in acetate buffer;

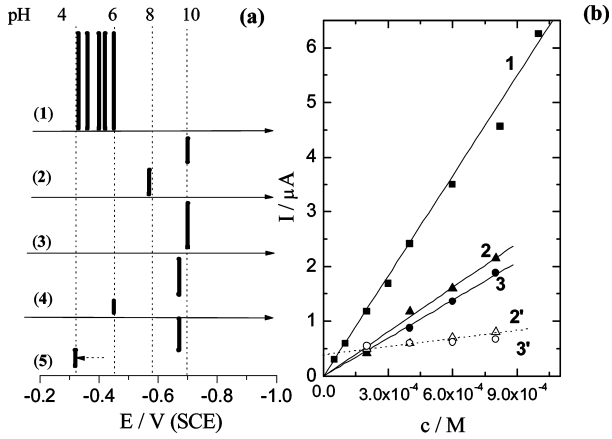

Figure 9. (a) Comparison of the data on electroreduction of 0.4 mM $[Cu_2L]Cl_2$ in (**1**) 0.1 M (mMOM + AcONa) pH 4.0−6.0, (**2**) 0.1 M AcONa (pH 8), (**3**) 0.1 M AcONa (pH 10.6), (**4**) 0.1 M NaF (pH 6.0), (**5**) 0.1 M KCl (pH 5.5). The lines refer to the half-wave potentials; dashed arrows denote the shift of potential from the value expected for the initial pH of solution. (b) Current vs $[Cu_2L]Cl_2$ concentration curves obtained at (1) −0.6 V (0.1 M acetate buffer pH 6); (2) −0.9 V, summarized currents (0.1 M AcONa), and (3) 0.9 V (0.1 M KCl). Currents of more profound $[Cu_2L]Cl_2$ reduction at (2′) −1.1 V (0.1 M AcONa) and (3′) −1.1 V (0.1 M KCl).

the slopes of these waves are 0.047 V (curve 2 in Figure 7) and 0.03 V (curve 1 in Figure 7), respectively.

The $[Cu_2L]Cl_2$ reduction in AN with different water content (i.e., with a possibility of $[Cu_2L]Cl_2$ protonation) was studied by cyclic voltammetry. When the amount of water in organic medium is low, the local pH effect should be more significant, as well as the corresponding shift of redox potential toward negative potential values. Qualitatively, this is in agreement with the experimental voltammograms in mixed solvents (Figure 8). The addition of water to AN results in the appearance of an additional peak at about −0.75 V in the cyclic voltammogram of $[Cu_2L]Cl_2$. The increase of water content in the mixture leads to a shift of this peak to more positive values of the potential (Figure 8).

(iv) Formulation of Problems for Model Analysis. The data on $[Cu_2L]Cl_2$ reduction in both buffered and nonbuffered media are summarized schematically in Figure 9. The lines in Figure 10a refer to the half-wave potentials. The height of the lines is proportional to the limiting current of the corresponding wave and, hence, to the number of consequently transferred electrons. The field **1** in Figure 9a describes the reduction of $[Cu_2L]Cl_2$ in acetate buffer accompanied with the consumption of protons ($1e^-/1H^+$). When $[Cu_2L]Cl_2$ is reduced in nonbuffered media (fields **2**, **3**, and **4** in Figure 9a), the polarograms demonstrate wave splitting. The potentials of reduction onset are consistent with the pH of the solutions (fields **2**, **4** in Figure 9a). When the more profound reduction takes place, the half-wave potential shifts to negative values and polarographic currents decrease. Each subsequent step of ET depends on the previous step because of local alkalization in the course of the one-electron reduction. To summarize the data on limiting currents, we will assume that the $[Cu_2L]Cl_2$ diffusion coefficients are equal or similar for protonated and deprotonated form.

For the $[Cu_2L]Cl_2$ reduction in chloride supporting electrolyte (field **5** in Figure 9a), the reduction onset is observed at the more positive potential compared to that expected for the initial pH of this solution. This shift of redox potential is marked by arrows in Figure 9a.

The sum of three waves' height in the region from 0 to −0.8 V in Figure 2b is about two times lower than the height of waves in Figure 2a for the same $[Cu_2L]Cl_2$ concentration. These estimates are rather approximate because of less pronounced steps at the curves in Figure 2b. Nevertheless, the height of the polarographic waves in the region from −0.4 to −0.9 V (line 2 in Figure 9b) demonstrates a linear dependence on the $[Cu_2L]Cl_2$ concentration. The slope of the lines in Figure 10b is associated with the number of electrons transferred in the reduction step. The slope of line 2 (Figure 9b) is twice as low as compared with that of line 1. As the line 1 relates to the four-electron $[Cu_2L]Cl_2$ reduction, one can suggest that the polarographic response at about −0.7 V (Figure 2b) results from a two-electron reduction. The same trends are observed for chloride solutions (line 3 in Figure 9b).

Finally, we summarize some observations, which call for a more detailed treatment and can be regarded as a challenge for computational modeling.

Concerning the results obtained for *purely acetate media* (Figure 2, subsection (i)), the main problem is the nature of the wave splitting resulting from the local pH increase. To model possible thermodynamic reasons of this situation, we need to compare the redox potentials E_1, E_2, E_1^{H+} and E_2^{H+} (Figure 1). The right branch gives no details on the protonation step, which can be preceding, concerted, or subsequent. This is a challenge for analysis of the elementary act of ET for protonated and deprotonated species.

As for the wave splitting in *nonaqueous media* (subsection (ii)), the modeling can be employed to compare an assumption of the local pH effect in the presence of water and an assumption of solvent effect on the redox potentials and rate constant of the subsequent single electron steps. Further, we limit ourselves to considering the reactant bonding with AN, as there is no serious difference in the behavior of reactant in various nonaqueous solvents.[12]

Finally, in relation to the earlier reduction in the presence of *chloride* (subsection (iii)), a model analysis of the competitive chloride and acetate bonding to the reacting species is of crucial importance, as well as consideration of ET from the adsorbed Cl anion to the complex.

There is no chance, unfortunately, to extract the rate constants from the polarographic data because the most interesting waves are highly reversible. Nevertheless, the role of protonation in ET kinetics and the mechanism of "chloride catalysis" are to be considered as qualitative kinetic problems. Concerning the latter problem, we will examine additionally the role of adsorption in the reactivity of binuclear complexes. Again, in the electrochemical system under study it is exceedingly complicated to attain reliable quantitative predictions using microscopic modeling. That is why we employ density functional theory (DFT) and modern quantum mechanical theories of charge transfer to elucidate first of all some important qualitative effects. Below we address key contributions to the reaction activation barrier, the electronic transmission coefficient, and estimate the standard redox

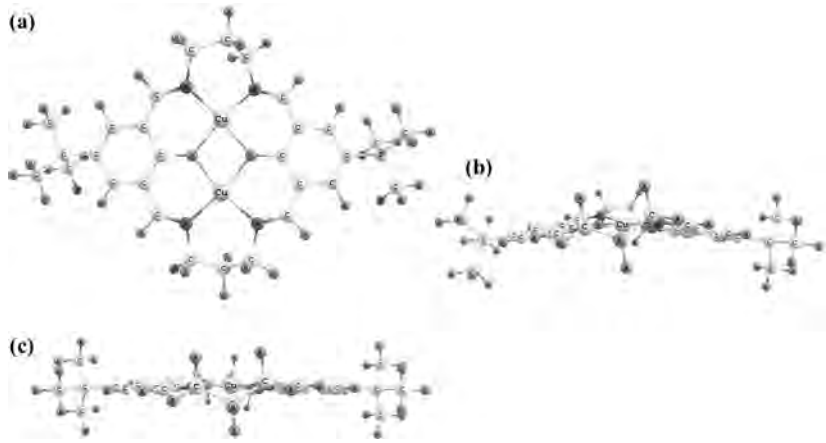

Figure 10. Optimized structure of Cu_2L^{2+} in oxidized (a, b) and mixed-valence Cu(I)−Cu(II) state (c).

Table 1. Selected Bond Lengths (nm) and Bond Angles (deg) Computed for Cu_2L^{2+} Using Three Different Basis Sets[a]

	from XRD[b]	Lanl2DZ	CEP-31 g	6−311+g(d)/6−31 g(d,p)
r(Cu−Cu)	0.3111	0.3094 (0.3219)	0.3103	0.309
r(Cu−N)	0.1971	0.201(0.202); 0.1987 (0.2025)	0.1988; 0.1971	0.199; 0.1974;
	0.1980	0.1991(0.202); 0.197 (0.2028)	0.1976; 0.1959	0.1979; 0.1963
r(Cu−O)	0.1988	0.199(0.2067); 0.198 (0.2061)	0.198	0.198
	0.1992			
∠ O−Cu−O	76.37	77.5 (77.3); 77.9 (77.4)	80.2−80.8	84.6−86.6
∠ N−Cu−N	96.43	98.6 (100.4); 97.3(100.4)	97.1; 98.7	98.5; 97.4

[a] Data for the Cu(II)−Cu(I) mixed valence state are given in parentheses. [b] Data for Cu_2L^{2+} solvate with chloroform from ref 20.

potentials. Emphasis will be put on a comparative study of different reactant forms and their orientations at the electrode surface.

III. Discussion

(i) Computational Details. Quantum chemical calculations of the Cu_2L^{2+} complex and certain adducts (including Cl^-, CH_3COO^- anions, and CH_3CN molecules in the coordination sheath) in oxidized and reduced forms were performed at the DFT level with the hybrid functional B3LYP as implemented in the Gaussian 03 program suite.[13] Nowadays quantum chemical methods resting on hybrid exchange-correlation functionals have became a powerful tool in studies of electronic structure and reactivity of various transition metal complexes (see, for example, ref 14). A basis set of double zeta (DZ) quality was employed to describe the valence electrons of Cu atom, whereas the effect of inner electrons was included in a relativistic effective core potential (LanL2) developed by Hay and Wadt. [15] The Dunning−Huzinaga valence basis set (D95V) was used to describe the electrons of O, N, C, Cl, and H atoms.[16] Several test calculations were done with the other basis sets: (a) 6−311+g(d) for the Cu atom and 6−31 g(d, p) for the O, N, C, and H atoms; (b) the Stevens-Basch-Krauss effective core potential (CEP)[17] and a basis set of DZ quality for all atoms. The open shell systems were treated in terms of unrestricted formalism. The geometry of complexes was fully optimized in the gas phase for the oxidized and reduced states without symmetry restrictions. The stability of Kohn−Sham orbitals was checked additionally.[13] For selected complexes the frequency calculations were calculated as well to ensure that the stationary points are minima. The solvation effects in the electrolyte bulk were addressed in the framework of the Polarizable Continuum Model (PCM)[18] as implemented in the Gaussian 98 package.[19] Values of 78.4 and 36.6 were taken as static dielectric constants for liquid water and AN, respectively. All calculations were run on dual CPU Pentium IV workstations.

(ii) Geometry and Electronic Structure of Cu_2L^{2+} Complex. The Cu_2L^{2+} electronic ground-state was found to be a triplet. Selected values of the bond lengths and valence angles are listed in Table 1. It can be argued that the geometry of the Cu_2L^{2+} complex is slightly sensitive to the different basis sets employed and agrees well with the experimental X-ray diffraction (XRD) data obtained for a $[Cu_2L]Cl_2$ crystalline salt. [20] As can be seen from Figure 10, the nearest coordination plane is twisted in the oxidized state of the complex (N−Cu−O−Cu dihedral angle values lie between 168° and 177°), which entails a noticeable bend of the macrocyclic polydentate ligand in agreement with the experimental data.[20] However, for the mixed-valence state (Cu(I)−Cu(II)) the geometry of ligand becomes noticeably flatter (see Figure 10); N−Cu−O−Cu dihedral angle values were computed to be 176−178°. This conspicuous feature

(13) Frisch, M. J.; Trucks, G. W.; Schlegel, H. B. et al.; *Gaussian 03*, Revision B.04; Gaussian, Inc.: Pittsburgh PA, 2003.
(14) (a) Niu, S.; Hall, M. B. *Chem. Rev.* **2000**, *100*, 353–405. (b) Siegban, P. E. M.; Blomberg, M. R. A, *Chem. Rev.* **2000**, *100*, 421–437.
(15) Hay, P. J.; Wadt, W. R. *J. Chem. Phys.* **1985**, *82*, 270–283.
(16) Dunning, T. H., Jr.; Hay, P. J. In *Modern Theoretical Chemistry*; Schaefer, H. F., III Ed.; Plenum: New York, 1976; Vol. *3*, p 1.
(17) Stevens, W.; Bash, H.; Krauss, J. *J. Chem. Phys.* **1984**, *81*, 6026–6033.
(18) Tomassi, J.; Mennucci, B.; Cammi, R. *Chem. Rev.* **2005**, *105*, 2999–3093.
(19) Frisch, M. J.; Trucks, G. W.; Schlegel, H. B. et al. *Gaussian 98*, Revision A.11.2; Gaussian, Inc.: Pittsburgh, PA, 2001.
(20) Roznyatovskiy, V. V.; Borisova, N. E.; Reshetova, M. D.; Ustinyuk, Yu. A.; Alexandrov, G. G.; Eremenko, I. L.; Moiseev, I. I. *Izv. Akad. Nauk, Ser. Khim.* **2004**, *6*, 1–10.

Table 2. Solvation Free Energy (ΔG_{solv}), the Effective Radius[a] (r_{eff}), and the Solvent Reorganization Energy (λ_s) Calculated for the First Electron Transfer to Cu_2L^{2+} in Two Different Media

			λ_s/eV		
solvent	$-\Delta G_{solv}$/eV	r_{eff}/nm	$x = 0.7$ nm	$x = 0.9$ nm	$x = 1.1$ nm
water	5	0.57	0.32	0.37	0.4
AN	4.1	0.7	0.22	0.26	0.3

[a] This quantity was estimated according to the approach suggested in ref 1a.

might be explained in terms of the spin population analysis made below.

The spin density (P_s) of paramagnetic Cu_2L^{2+} complex resides mostly on the $3d_{x^2-y^2}$ orbitals of the Cu atoms ($P_s(Cu) = 0.6$) and their nearest surrounding atoms ($P_s(N) = 0.13$ and $P_s(O) = 0.14$). In the mixed-valence state the spin density of the central fragment is significantly reduced: $P_s(Cu) = 0.3$, $P_s(N_1) = 0.04$, $P_s(N_2) = 0.08$, $P_s(O_1) = 0.03$, and $P_s(O_2) = 0.15$. Because the $^{N}_{N}$>Cu<$^{O}_{O}$>Cu<$^{N}_{N}$ fragment has no π-bond which would enable it to stabilize in a flat position, Coulombic repulsion between the nitrogen and oxygen atoms imposes a tetragonal-like coordination of the copper atom. On the other hand, the repulsion effect is smaller in the mixed-valence state and most likely cannot result in a noticeable distortion of the square-flat coordination of Cu atoms.

The geometry of a model complex $Cu_2L(H_2O)_4^{2+}$ has also been also optimized to examine a possible effect of water molecules from the nearest coordination sheath of Cu_2L^{2+}. The four water molecules are bound to the copper atoms in axial position. As expected, no significant chemical interaction was observed, most likely because of the repulsion between the fully occupied $3d_{z^2}$ orbital of the Cu atoms and the lone electron pairs of the H_2O molecules. The Cu−H_2O bond length values are larger as compared with those of the Cu−O and Cu−N bonds (Table 1) and amount to 0.24−0.26 nm. We did not observe any noticeable influence of these axially bound water molecules on the geometry of Cu_2L^{2+}; that is why they were neglected in further calculations.

For a simplified analysis of the reaction layer, the Cu_2L^{2+} complex might be treated as a conducting ellipsoid. We suggest a simple way to choose the ellipsoid semiaxes (a, b, c) values. First, they should obey some evident geometry restrictions which stem from the shape of the particle. Second, the following equation should be fulfilled[21]

$$\Delta G_{solv} = (1 - 1/\varepsilon)\frac{q^2}{4}\int_0^\infty \frac{d\xi}{\sqrt{(\xi + a^2)(\xi + b^2)(\xi + c^2)}} \quad (2)$$

where ΔG_{solv} is the solvation energy of a particle bearing charge q; ε is the dielectric constant of the solvent.

We computed ΔG_{solv} using the PCM (see subsection (i)), which employs a nonspherical cavity formed by overlapping atom-centered spheres surrounding a particle in a dielectric medium. For aqueous solutions ($\Delta G_{solv} = 5$ eV, see Table 2) the best choice for the a, b, and c values was found to be 0.85, 0.57, and 0.28 nm, respectively. For AN ($\Delta G_{solv} = 4.1$ eV) the values obtained were larger as follows $a = 0.96$ nm, $b = 0.68$ nm, and $c = 0.39$ nm.

In the next section the computational results will be used to estimate key contributions to the activation barrier of the Cu_2L^{2+} electro-reduction and the electronic transmission coefficient.

(iii) Franck−Condon Barrier and Electronic Transmission Coefficient. For ET reactions the Franck−Condon (FC) barrier (ΔE_{FC}) constitutes a main part of the activation energy. According to the Marcus theory[22] the simplest equation for the ΔE_{FC} of interfacial ET can be written as follows,[23]

$$\Delta E_{FC} = \frac{(\lambda_r - F\eta)^2}{4\lambda_r} \quad (3)$$

where λ_r is the total reorganization energy commonly split into contributions from solvent (λ_s) and intramolecular degrees of freedom (λ_{in}); η is the electrode overpotential.

The Marcus formula[22] is frequently employed to calculate the solvent reorganization energy,

$$\lambda_s = Ce_0^2\left\{\frac{1}{2r_{eff}} - \frac{1}{4x}\right\} \quad (4)$$

where C is the Pekar factor ($C = 1/\varepsilon_{opt} - 1/\varepsilon_{st}$, ε_{opt} and ε_{st} are the optical and static dielectric constants of polar liquid);[24] r_{eff} is the effective radius of reactant; x is the reactant center-electrode surface distance.

Because Cu_2L^{2+} is nonspherical, it is more reasonable to use an extended version of eq 4,

$$\lambda_s = C\frac{e_0^2}{4}\left(\int_0^\infty \frac{d\xi}{\sqrt{(\xi + a^2)(\xi + b^2)(\xi + c^2)}} - \frac{1}{x}\right) \quad (5)$$

where a, b, and c are the semiaxes of a model ellipsoid describing the reactant (see subsection (ii)).

The λ_s values were multiplied by a factor of 0.8 to address quantum degrees of freedom of the solvents.[25,26] Note that the "orientational" effects on the λ_s values in the terms of eq 3 can be treated taking different x values which differ apparently for different orientations of the reactant relative to the electrode surface (Figure 11). The results of the calculations are summarized in Table 2.

The λ_s values were found to be larger for water as compared with AN. They are slightly dependent on the reactant-electrode distance x. In the region 0.5 nm < x < 1.1 nm, the solvent reorganization energy varies from 0.27 to 0.4 eV.

Equations 4 and 5 presume a local dielectric response of the solvent. In general, the solvent reorganization can be

(21) This equation can be treated as extension of the Born model for a charged spherical particle; we employ the well-known formula for the potential of the surface of a charged conducting ellipsoid immersed in a dielectric medium.

(22) Marcus, R. A. *J. Chem. Phys.* **1965**, *43*, 679–701.

(23) We neglect for simplicity the work terms of reactant and product, as well as a manifold of electron energy levels in a metal electrode which could change the reaction free energy.

(24) The Pekar factor values for liquid water and AN do not differ much from each other (0.56 and 0.53, respectively).

(25) Kuznetsov, A. M. *Charge Transfer in Physics, Chemistry and Biology. Mechanism of Elementary Processes and Introduction to the Theory*; Gordon and Breach: Berkshire, 1995.

(26) Kuznetsov, A. M.; Ulstrup, J. *Electron Transfer in Chemistry and Biology*; John Wiley&Sons, Inc.: Chichester, 1999.

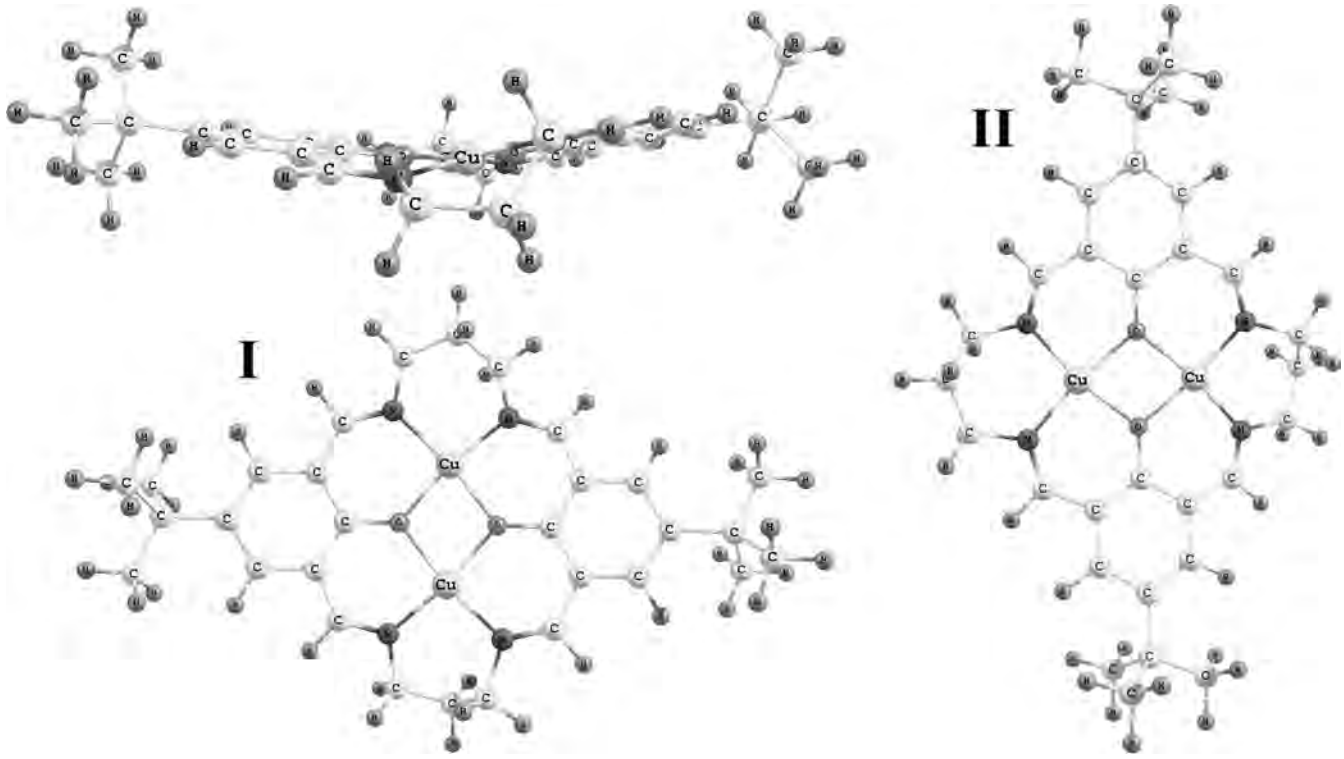

Figure 11. Three different orientations of Cu_2L^{2+} relative to the electrode surface (planar, vertical I, II), which is assumed to be at the bottom of the figure.

Table 3. Intra-Molecular Contribution ($\tilde{\lambda}_{in}$/eV) to the Total Reorganization Energy Computed for Reduction of Different Complex Forms[a]

$Cu_2L^{2+/+}$	$Cu_2LCl^{+1/0}$	$Cu_2LCl_2^{0/1-}$	$Cu_2L(Ac)_2^{0/1-}$	$Cu_2L(AN)_2^{2+/+}$
0.21 (0.22[b]; 0.19[c])	0.32	0.41	0.44	0.29

[a] $\tilde{\lambda}_{in}$ is the averaged inner sphere reorganization energy defined by the following way,[1b] $\tilde{\lambda}_{in} = 4\vec{\lambda}_{in}\overleftarrow{\lambda}_{in}/(\sqrt{\vec{\lambda}_{in}} + \sqrt{\overleftarrow{\lambda}_{in}})^2$; $\vec{\lambda}_{in}$ and $\overleftarrow{\lambda}_{in}$ refer to the reduction and oxidation processes, respectively. [b] 6−311+g(d)/6−31 g(d,p) basis sets. [c] CEP-31 g basis set.

addressed on the basis of nonlocal electrostatics, where certain dependencies of ε on the wave vector k are considered (see, for example, ref 27 for heterogeneous ET). It should be noted that nonlocal solvent effects are noticeable, first of all, for reactants of small size.

The first ET entails some reorganization of the inner-sphere environment of copper atoms; the relevant data are collected in Table 1. The averaged intramolecular contributions ($\tilde{\lambda}_{in}$) to the FC barrier were computed as a difference in the total energies of oxidized and reduced species in equilibrium and nonequilibrium states (Table 3). A value of 0.2 eV has been obtained for Cu_2L^{2+} which is noticeably smaller as compared with the solvent reorganization energy. The dominant contribution to $\tilde{\lambda}_{in}$ comes from the reorganization of Cu−O bonds and dihedral angles. The model predictions on both the geometry change and $\tilde{\lambda}_{in}$ values made for the $Cu_2L^{2+/+}$ redox pair do not depend strongly on the basis set employed (see Table 3).

This approach can be justified, if the reorganization of intramolecular quantum modes ($\hbar\omega \gg kT$) is small. Otherwise, the FC barrier might be overestimated, since such modes affect the reaction rate mostly through a tunneling factor. According to our results, the change of the C−H, C−C, C−N, and C−O bond lengths and of the corresponding valence angles at the reduction of Cu_2L^{2+} does nor exceed 0.001 nm and 1 degree, respectively. Hence, a small reorganization of the quantum degrees of freedom practically does not affect the accuracy of our estimations.

Another quantity which also plays a crucial role in the ET kinetics is the electronic transmission coefficient (k_e). If a metal electrode participates in ET, we have to deal with a manifold of crossing free energy surfaces (FES) describing the initial and final states of a redox pair. No analytical formula to calculate k_e for such a system was devised so far; the results of pertinent Monte Carlo simulations have been reported in ref 28. That is why we restrict ourselves to an estimate in the framework of the Landau−Zener (LZ) theory which presumes two crossing FES and takes into account only direct ballistic trajectories,[25,26]

$$\kappa_e \approx 1 - \exp(-2\pi\gamma_e) \tag{6}$$

If the intramolecular reorganization can be treated in the harmonic approximation, the LZ factor γ_e in eq 6 takes the form,[25,26]

$$\gamma_e \approx N_{eff}\frac{V_{if}^2}{\hbar\omega}\sqrt{\frac{\pi}{(\lambda_s + \tilde{\lambda}_{in})kT}} \tag{7}$$

where N_{eff} is the number of electrons contributing to the ET act (for the region of small electrode overpotentials $N_{eff} \approx \rho(\varepsilon_F)\ kT$, where $\rho(\varepsilon_F)$ is the density of electronic states at the Fermi level of a metal electrode); ω is the effective polarization frequency of liquid water ($\approx 10^{13}$ c^{-1});[25] V_{if} is

(27) Medvedev, I. G. *J. Electroanal. Chem.* **2001**, *517*, 1–14.
(28) Kuznetsov, A. M.; Nazmutdinov, R. R.; Schmickler, W. *J. Electroanal. Chem.* **2002**, *532*, 171–180.

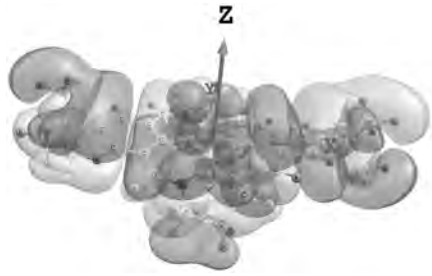

Figure 12. Acceptor orbital of Cu_2L^{2+}.

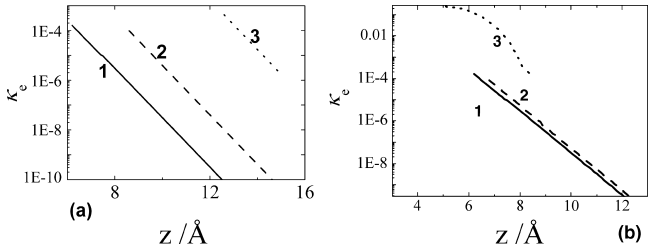

Figure 13. (a) Electronic transmission coefficient (k_e) as a function of the Cu_2L^{2+} center electrode distance (z) computed for different Cu_2L^{2+} orientations: (1) planar, (2) vertical I, (3) vertical II. (b) mM vs z calculated for (1) $[Cu_2L]^{2+}$, (2) Cu_2LCl_2 adduct, and (3) configuration $Cl^-_{ads}-Cu_2L^{2+}$.

the one-electron matrix element.

The most important quantity in eq 7, which governs the order of the LZ factor, is V_{if}. We estimated the latter using perturbation theory,

$$V_{if} = \int \psi_i \hat{V} \psi_f \, d\Omega \tag{8}$$

where ψ_i is the wave function of a metal electrode; ψ_f is the highest occupied molecular orbital of the reactant in a reduced state (i.e., the electronic relaxation effect is taken into account); $\hat{V}$ is a perturbation potential resulting in the ET.

The operator $\hat{V}$ was constructed using the molecular potential of the complex in the initial (oxidized) state screened by the dielectric response of the medium. The jellium model was employed to address the electronic properties of a metal electrode. Pertinent details of the calculation of V_{if}, as well as critical comments on this model approach have been reported earlier in ref 29. The distance-dependent k_e values were computed for three different orientations of the complex reactant relative to the electrode surface (Figure 11). The results are shown in Figure 12 and can be fitted to the form,

$$\kappa_e = \kappa_0 \exp(-x/\beta) \tag{9}$$

where β takes on values of 0.0444, 0.0437, and 0.0434 nm, for "planar", "vertical I", and "vertical II" orientations, respectively.

Lower x values, for which the fit given by eq 9 is still valid, are restricted to the values of ellipsoid semiaxes for a given orientation. The nearly similar slopes of the k_e versus x dependencies can be explained by the strongly delocalized character of the highest occupied molecular orbital (HOMO) of Cu_2L^+ (Figure 13); the main contribution to this orbital comes from the aromatic rings of the ligand. The ET proceeds in the diabatic regime for all orientations ($k_e \ll 1$). We have to stress again the qualitative character of our model predictions which originate from the approximations made for the matrix element V_{if}. It has been recently attempted only a few times to calculate the electronic transmission coefficient for interfacial ET reactions in the framework of a quantum mechanical theory.[29a,30] Quantum chemical calculations of V_{if} with higher accuracy for certain homogeneous redox pairs were also reported in ET literature.[31]

The data on electronic transmission coefficient values discussed above can hardly be used in an unambiguous way without additional information about the reaction layer (first of all, the distances of closest approach, x_0). The x_0 values may be obtained from the minima of potential energy surfaces describing the interaction of Cu_2L^{2+} with the electrode. As DFT calculations of such energy profiles present an exceedingly difficult and computer time demanding problem, we restricted ourselves to rough estimations based on the semiempirical PM3 method parametrized for transition elements as implemented in the HyperChem 7.0 program suite. The mercury surface was described as a planar Hg_{19} cluster (see some details in ref 32). The geometry of the Cu_2L^{2+} complex was fixed as obtained by the previous DFT calculations, while the complex−Hg surface distance (x) was scanned. The spin multiplicity of the adsorption complex was taken as 3 (see section (ii)); the nonrestricted Hartree−Fock formalism was employed. Using this model we have obtained values of 0.6 nm ("planar" orientation) and 1 nm ("vertical I") for x_0 reckoned from the mercury "edge" (see also relevant discussion if ref 29c). As follows from our calculations, the mercury cluster−complex interaction energy is stronger for the "planar" orientation. If a reasonable range of 0.35−0.4 nm is assumed for the position of the outer Helmholtz plane (OHP), we can argue that the complex reactant resides mostly outside the OHP and does not penetrate into the compact part of electrical double layer (i.e., at least a monolayer of water molecules remain between the reactant and electrode surface). In other words, an energy loss required for desorption of water molecules can be neglected and the direct Cu_2L^{2+}−electrode interaction does play the most important role. Thus, the "planar" position of Cu_2L^{2+} looks more favorable compared to the other orientations. It is also evident that repulsive interactions between Cu_2L^+ complexes in a "planar" position are smaller than for both vertical orientations.

So far, only one intermediate, Cu_2L^+, was considered in our model calculations. In the next section we extend this

(29) (a) Nazmutdinov, R. R.; Glukhov, D. V.; Tsirlina, G. A.; Petrii, O. A. *Russ. J. Electrochem.* **2003**, *39*, 97–107. (b) Nazmutdinov, R. R.; Glukhov, D. V.; Petrii, O. A.; Tsirlina, G. A.; Botukhova, G. N. *J. Electroanal. Chem.* **2003**, *552*, 261–278. (c) Nazmutdinov, R. R.; Schmickler, W.; Kuznetsov, A. M. *Chem. Phys.* **2005**, *310*, 257–268.
(30) (a) Hsu, C.-P.; Markus, R. A. *J. Chem. Phys.* **1997**, *106*, 584–598. (b) Gosavi, S.; Gao, Q.; Marcus, R. A. *J. Electroanal. Chem.* **2001**, *500*, 71–77. (c) Smalley, J. F.; Sanchs, S. B.; Chidsey, C. E. D.; Dudek, S. P.; Sikes, H. D.; et al, *J. Am. Chem. Soc.* **2004**, *126*, 14620–14630.
(31) (a) Logan, J.; Newton, M. D. *J. Chem. Phys.* **1983**, *78*, 4086–4091. (b) Newton, M. D. *J. Phys. Chem.* **1991**, *95*, 30–38. (c) Newton, M. D. *Chem. Rev.* **1991**, *91*, 767–792. (d) Endres, R. G.; LaBute, M. X.; Cox, D. L. *J. Chem. Phys.* **2003**, *118*, 8706–8714. (e) Kennepohl, P.; Solomon, E. *Inorg. Chem.* **2003**, *42*, 696–708. (f) Rosso, K. M.; Smith, D. M. A.; Dupuis, M. *J. Phys. Chem. A.* **2004**, *108*, 5242–5248.

Table 4. Protonation Enthalpy (ΔH_p/eV) Estimated for Several Model Reactions Occurring in Two Different Solvents[a]

model processes	water	AN
$Cu_2L^{2+} \xrightarrow{H^+} Cu_2LH^{3+}$	1.0	1.1
$Cu_2L^{+} \xrightarrow{H^+} Cu_2LH^{2+}$	0.25	0.05
$Cu_2L^{+} \xrightarrow{2H^+} Cu_2LH_2^{3+}$	1.01	0.9
$Cu_2LH^{+} \xrightarrow{H^+} Cu_2LH_2^{2+}$	−0.12	−0.26

[a] Values of −11.095 eV and −10. 77 eV were taken for solvation energy of proton in water and AN, respectively[37].

to a number of possible intermediate forms to explore some microscopic aspects of the protonation effect.

(iv) Effect of Protonation. Let us consider two different routes (Figure 1) of the sequential electroreduction of Cu_2L^{2+},

$$Cu_2L^{2+} + e^- \rightarrow Cu_2L^{+} + e^- \rightarrow Cu_2L^{0} \qquad (9a)$$

and

$$Cu_2L^{2+} + e^- \xrightarrow{H^+} Cu_2LH^{2+} + e^- \xrightarrow{H^+} Cu_2LH_2^{2+} \qquad (9b)$$

The second route involves the protonation of intermediates (the rate of this process is assumed to be very fast).[33]

We have performed DFT calculations of different protonated forms of Cu_2L^{2+} (both for oxidized and reduced states): Cu_2LH^{3+}, Cu_2LH^{2+}, $Cu_2LH_2^{3+}$ and $Cu_2LH_2^{2+}$. Note that experimental data give evidence in favor of either O or N atoms as possible protonation centers.[34] We found that for both Cu_2L^{2+} and Cu_2L^{+} complexes the partial charge of the O atoms (−0.8 e (ox); −0.72 to −0.74 e (red)) is more negative compared to that of the nitrogen atoms (−0.5 to −0.53 e (ox, red)).[36] This might favor the protonation of oxygen atoms (O*). Moreover, as shown by means of additional calculations, protons attached to the O* atoms exhibit a stronger interaction with a nearest water molecule than the protonated N atoms (N*). According to our results the O*−OH_2 bond length amounts to 0.252 nm while a larger value of 0.27 nm was observed for r(N*−OH_2). In further calculations we considered the oxygen atoms as the model protonation centers. The optimized geometry of the complexes was used to address the solvation effects in water and AN on the basis of PCM.

Estimates of the protonation enthalpy (ΔH_p) for several model processes are reported in Table 4. The computational results predict large positive ΔH_p) values for the protonation of Cu_2L^{2+} in the both solvents and, therefore, point to its small probability. In contrast, the formation of a protonated Cu_2LH^{2+} complex from an intermediate product Cu_2LH^{+} looks more probable (especially for AN). The further protonation of a reduced form of Cu_2LH^{2+} leads even to negative ΔH_p) values and was found to be the most feasible. The optimized structure of Cu_2LH^{2+} and $Cu_2LH_2^{2+}$ intermediates is displayed in Figure 14. A noticeable lengthening of Cu−O* bonds compared to Cu_2L^{+} (see Table 1) is observed for Cu_2LH^{2+}: r(Cu−O*) = 0.227 nm; 0.229 nm. The second intermediate $Cu_2LH_2^{2+}$ exhibits a more significant distortion leading practically to the break of two Cu−O* bonds: r(Cu_1−O*) = 0.216 nm; 0.267 nm and r(Cu_1−O*) = 0.213 nm; 0.27 nm. Although the computational level is not enough to provide complete quantitative accuracy, the differences should be reliable. As a next step we examine the influence of protonation on relevant redox potentials.

For aqueous solutions the standard redox potential reckoned from the hydrogen electrode (E_0) was computed as follows,

$$E_0 = -zF\Delta\vec{F} - 4.34 \qquad (10)$$

where $\Delta\vec{F}$ is the free energy of the reduction process; z is the number of electrons transferred.

In eq 10 the value of −4.34 eV refers to the free energy of the reaction $H^+_{(aq)} \rightarrow {}^1/_2H_{2(aq)}$ (see, for example, ref 38). The reaction free energy was estimated as a difference of the total energies of complexes including the solvation contribution. The latter, in turn, consists of electrostatic and nonelectrostatic parts. The nonelectrostatic component (sum of cavitation, dispersion, and repulsion energies) was calculated to contribute noticeably to the solvation free energy, mainly because of the large size of complexes. For aqueous solution this contribution increases in the range 8−37% going from $[Cu_2L]^{2+}$ to $[Cu_2L]$.

To predict the redox behavior of $[Cu_2L]^{2+}$ taking into account the protonation of its intermediate product (route ***b***), we can compare the difference of redox potentials of two consecutive one-electron reduction steps (see Table 5). This difference in the absence of protons ($E_0^{(1)}$ and $E_0^{(2)}$) amounts to about 1 V and exceeds significantly an estimate of 0.08 V ($^{H}E_0^{(1)}$ and $^{H}E_0^{(2)}$) obtained assuming protonation. This result is in qualitative agreement with the experimental data if route ***a*** for nonbuffered and route ***b*** for buffered solutions are considered.

A further insight into the effect of protonation on the reaction mechanism can be gained by exploring the diabatic FES which describe a multistep ET. Because for the full electroreduction of $[Cu_2L]^{2+}$ the construction of such surfaces is rather complicated, we restrict ourselves to the modeling of two ET stages (routes ***a*** and ***b***). For this particular case a three-dimensional surface along the dimensionless solvent (q) and inner-sphere (q_{in}) coordinates,E(q,q_{in}), can be built using an approach based on the Anderson model Hamiltonian.[39,40] An equation for $E(q,q_{in})$ is recast in the form,

(32) Borzenko, M. I.; Nazmutdinov, R. R.; Glukhov, D. V.; Tsirlina, G. A.; Probst, M. *Chem. Phys.* **2005**, *319*, 200–209.
(33) Investigation of other intermediates arising due to the third ET step is out of the scope of this work.
(34) Borisova, N. E.; Reshetova, M. D.; Yustynyuk, Y. A. *Chem. Rev.* **2007**, *107*, 46–79.
(35) Brenerman, C. M.; Wiberg, K. B. *J. Comput. Chem.* **1990**, *11*, 361–373.
(36) The ChelpG scheme,[35] which gives the best fit of molecular potential, was employed to compute the atomic charges.
(37) Ismailov, N. A. *Doklady Akad. Nauk SSSR* **1963**, *149*, 1364.
(38) Remita, S.; Archirel, P.; Mostafi, M. *J. Phys. Chem.* **1995**, *99*, 13198–13202.
(39) Anderson, P. W. *Phys. Rev.* **1961**, *124*, 41–53.
(40) Schmickler, W. *Chem. Phys. Lett.* **1995**, *237*, 152–160.

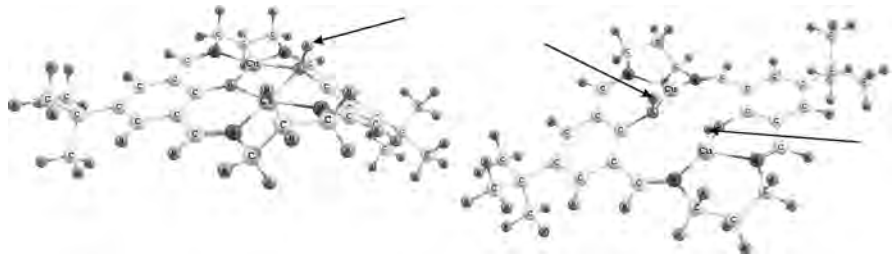

Figure 14. Optimized structure of certain protonated intermediates: (a) $[Cu_2LH]^+$; (b) $[Cu_2LH_2]^{2+}$.The arrows indicate the protons bound to the O atoms.

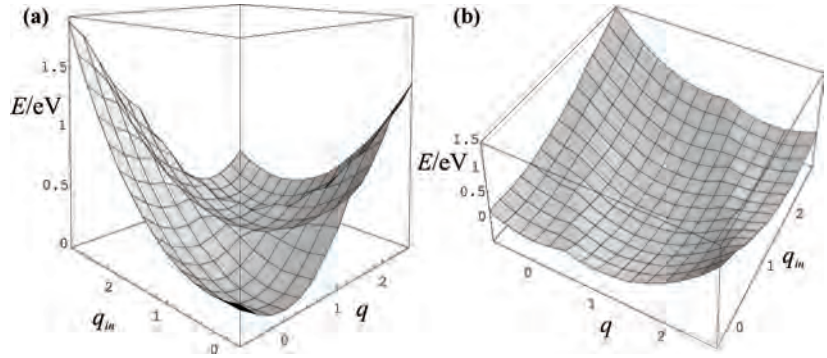

Figure 15. FES built along the solvent (q) and intramolecular (q_{in}) reaction coordinate for the two-step ET constructed at zero electrode overpotential; $\lambda_s = 0.4$ eV, $\lambda_{in} = 0.2$ eV ((a) $U^* = 0.8$ eV; (b) $U^* = 1.9$ eV).

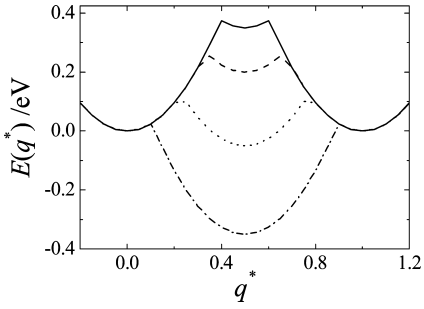

Figure 16. Section of the reaction free energy surface (E) along a line connecting two minima related to the initial and final state (q^*) constructed at zero electrode overpotential; $\lambda_s = 0.4$ eV, $\lambda_{in} = 0.2$ eV, $U^* = 0.5$ eV (solid), $U^* = 0.8$ eV (dashed), $U^* = 1.3$ eV (dotted), $U^* = 1.9$ eV (dashed-dotted).

$$E(q, q_{in}) = \sum_{\sigma} \tilde{\varepsilon}_{\sigma} y_{\sigma} - U y_{\sigma} y_{-\sigma} + \lambda_s q^2 + \lambda_{in} q_{in}^2 \qquad (11)$$

where y_σ and $\tilde{\varepsilon}_\sigma$ denote the occupation probability of the indicated spin state (σ, $-\sigma$) and the effective energy level of the reactant; U is the Coulomb integral describing the repulsion of the electrons at an effective reactant orbital; λ_s and λ_{in} are the solvent and inner-sphere reorganization energies related to the transfer of the first electron.

The effective energy level of reactant is defined as follows (the Hartree−Fock theory is assumed to describe the electron−electron repulsion):[39,40]

$$\tilde{\varepsilon}_{\sigma}(y_{-\sigma}, q, q_{in}) = \varepsilon_0(\eta) + U y_{-\sigma} - 2\lambda_s q - 2\lambda_{in} q_{in} \qquad (12)$$

where η is the electrode overpotential; ε_0 is the energy parameter which is responsible for equalizing with the minima of the FES related to the initial (reactant) and final (product) states at $\eta = 0$, as well as for the changing of shape of the energy surface when $\eta > 0$.

The equations for the occupation probability in the "wide band" approximation[38] take the form

$$\begin{cases} y_{\sigma} = \dfrac{1}{\pi}\operatorname{arc\,cot}\left\{\dfrac{\tilde{\varepsilon}_{\sigma}(y_{-\sigma}, q, q_{in})}{\Delta}\right\} \\ y_{-\sigma} = \dfrac{1}{\pi}\operatorname{arc\,cot}\left\{\dfrac{\tilde{\varepsilon}_{-\sigma}(y_{\sigma}, q, q_{in})}{\Delta}\right\} \end{cases} \qquad (13)$$

where Δ is the coupling parameter (Δ is proportional to the square of the electronic matrix element).[39] We solved these equations using an effective computational scheme developed recently in ref 41.

Then, the activation energy barriers (ΔE_a) can be calculated as the energies of $E(q,q_{in})$ saddle points reckoned from their minimum values (related to the initial or intermediate states of the reaction system). In our limiting case with $\Delta < kT$ (a value of 0.01 eV was taken in the calculations), the FES barriers are of cusp-like form, and the reactant-electrode overlap practically does not affect the ΔE_a values. Thus, only three parameters,λ_s, λ_{in}, and U fully define the shape of the FES at small overpotential values. In general, a FES described by eq 11 has three minima separated by two energy barriers (saddle points). However, if $U \rightarrow 0$, the FES exhibits only one energy barrier. Oppositely, at large U values two energy barriers can disappear and the FES resembles more a pit. The approach developed in ref 40 was employed to study various adiabatic multistep ET reactions occurring at electrochemical interfaces (see, for example, ref 42).

The Coulomb integral U was estimated as the difference between two quantities, δE_2 and δE_1. For route ***a*** $\delta E_1 = E_{tot}(Cu_2L^+) - E_{tot}(Cu_2L^0)$ and $\delta E_2 = E_{tot}(Cu_2L^{2+}) - E_{tot}(Cu_2L^+)$; the geometry of the complex was taken to be that of Cu_2L^0 (δE_1 and δE_2 can be interpreted as the first and the second ionization potentials related to Cu_2L^0). Because for route ***b*** the proton attachment to Cu_2L^+ occurs additionally in the elementary step, $\delta E_1 = E_{tot}(Cu_2LH^{2+}) -$

$E_{tot}(Cu_2LH^+)$, while δE_2 was calculated as described above. The U values were found to be 3.72 eV (***a***) and 1.2 eV (***b***), see Supporting Information, Table 6. It has to be kept in mind that the Coulomb repulsion of electrons in the effective orbital of the reactant is reduced by the effect of quantum solvent modes and plasmons (collective exitations) induced in a metal electrode. We have taken into account the influence of fast solvent modes when computing $\delta E_{1(2)}$ values by assuming a value of 1.8 for the dielectric constant describing water in the solution bulk in terms of the PCM. The influence of plasmons on U was addressed as follows:

$$U^* = U - 2\left|V_{im}\right| \tag{14}$$

where the V_{im} image term describes the interaction of an electron in the acceptor orbital of the reactant with plasmons. As was shown in ref 43,

$$V_{im}(x) \approx -e_0^2 \frac{\sqrt{2}\omega_p}{4\tilde{v}_{||}} K_0\left(\sqrt{2}\omega_p x/\tilde{v}_{||}\right) \tag{15}$$

where ω_p is the plasmon frequency (a value of $\approx 3 \times 10^{16}$ s^{-1} was obtained for mercury on the basis of the free electron gas model); $v_{||}$ is the longitudinal component of the average velocity of the electron and was estimated using a value of 20 eV for the kinetic energy of the electron in the Cu_2L^+ HOMO orbital).

The results of our calculations are compiled in Supporting Information, Table 7. It can be seen that the U^* values fall in the intervals 3.06−3.42 eV (a) and 0.54−0.9 eV (b) for x ranged from 0.5 to 0.9 nm. The typical FES describing the two-step ET and constructed at two different U^* values are plotted in Figure 15; the sections of a family of the different reaction FES are also shown in Figure 16. As expected, small U^* values entail a noticeable decrease of the second FC barrier. At $U^* = 0.5-0.8$ eV the second ET proceeds significantly faster than the first one and the whole reaction can be treated as an effective one-step process. Such a FES might appear when the reaction takes place in accordance with route ***b***. In contrast, when increasing U^*, both FC barriers gradually decrease and the FES sections turn into a deep pit. This can be interpreted as the formation of a large activation barrier on the path of the second ET. This limiting case might be attributed to the route ***a*** (large U^* values).

More rigorous computational schemes with exact treatment of the electron correlation should be mentioned too.[44,45] The results of our test calculations based on the "surface molecule" model[44] confirm qualitatively the FES shape for both **a** and ***b*** routes.

It should be noted, however, that the free energy surface fully controls the ET kinetics only for adiabatic reactions. In the diabatic limit the rate of i-th ET step, $k_s^{(i)}$, can be written in the form

$$k_s^{(i)} = \frac{\omega}{2\pi}\kappa_e^{(i)} \exp\left(-\Delta E_a^{(i)}/kT\right) \tag{16}$$

Therefore, one needs estimations of both the activation barriers, $\Delta E_a^{(i)}$, and the electronic transmission coefficients, $\kappa_e^{(i)}$, to judge about the limiting reaction step. It follows from our calculations performed for the planar orientation (see Figure 11) that $\kappa_e^{(i)}$ values for Cu_2L^+ (the second ET) are noticeably less as compared with Cu_2L^{2+} (the first ET). For Cu_2L^{2+} the κ_0 and β values (see eq 9) are 61.674 and 0.0444 nm, whereas for Cu_2L^+ these model parameters are 0.084 and 0.0465 nm, respectively. For the protonated form Cu_2LH^{2+} we obtained, on the other hand, the κ_e values (κ_0 = 3.575 and β= 0.0448 nm) which exceed those for Cu_2L^+. As for the orientation "vertical I", our model calculations predict close κ_e values for Cu_2L^+ and Cu_2LH^{2+}. Therefore, the pre-exponential factors do not change the conclusions on the reactivity of the protonated form made above.

To summarize this subsection, one should emphasize that both the estimates of redox potentials and the model FES point to the crucial role of protonation of intermediates at the Cu_2L^{2+} electro-reduction. Thermodynamics favors a higher difference of potentials for the first and second step in the absence of protonation (route ***b***), and simultaneously kinetics favors simultaneous transfer of two electrons under protonation conditions. The combination of these two features is needed to explain the experimentally observed merging of single electron waves in nonbuffered aqueous media which do not support protonation.

(v) Effect of the Solvent. The redox potentials were also estimated for AN solutions. The standard potential of a redox pair in AN cannot be defined similar to eq 10 because of the absence of a commonly adopted reference electrode in nonaqueous media. This is not a serious complication because we are interested, first of all, in comparative estimations of potentials for redox systems involving or not involving the proton, as well as in comparison of potentials for subsequent redox steps. In AN, the nonelectrostatic part plays a more important role than in aqueous media; for example, it constitutes half of the solvent free energy. The additional (translation, rotational, and vibration) entropy terms were found to be small and alter only slightly the above mentioned estimates.

The difference of potentials for the first and second single electron redox transition corresponding to routes ***a*** and ***b*** (left and right branches in Figure 1) for AN were estimated to be 1.4 V (without protons) and 0.58 V (with protonation). Although this difference is qualitatively the same as reported above for aqueous medium, we cannot use this result for the direct interpretation of the experimental data. The main complication in a comparison of experimental and computational results originates from a possible presence of water in the reactant in mixed AN−water medium (see Introduc-

(41) Bronshtein, M. D.; Nazmutdinov, R. R.; Schmickler, W. *Chem. Phys. Lett.* **2004**, *399*, 307–314.
(42) (a) Boroda, Yu. G.; Voth, G. A. *J. Electroanal. Chem.* **1998**, *450*, 95–107. (b) Koper, M. T. M.; Schmickler, W. *J. Electroanal. Chem.* **1998**, *450*, 83–94. (c) Nazmutdinov, R. R.; Zinkicheva, T. T.; Tsirlina, G. A.; Kuz'minova, Z. V. *Electrochim. Acta* **2005**, *50*, 4888–4896.
(43) Brodskii, A. M.; Urbakh, M. I. *Electrodynamics of a metal/electrolyte solution interface* (in Russian); Nauka: Moscow, 1989.
(44) Kuznetsov, A. M.; Medvedev, I. G. *J. Electroanal. Chem.* **2001**, *502*, 15–35.
(45) Kuznetsov, A. M.; Medvedev, I. G.; Sokolov, V. V. *J. Electroanal. Chem.* **2003**, *552*, 231–246.

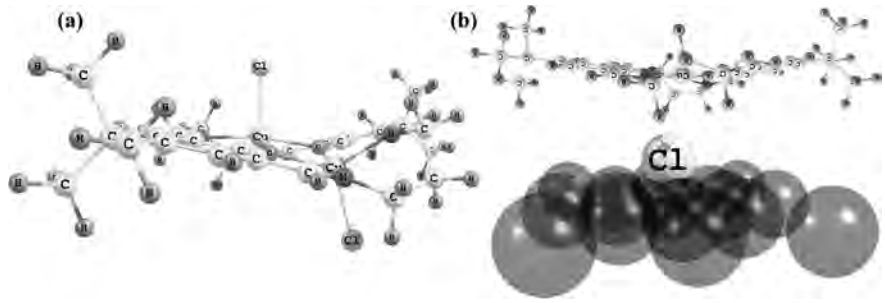

Figure 17. Optimized structure of $[Cu_2LCl_2]$ (a); (the most favourable configuration for ET in the adsorption complex $Cl^-_{ads} - Cu_2L^{2+}$ (b).

Table 5. Standard Redox Potentials (V) Calculated for Several Model Processes in Aqueous Solutions

Cu_2L^{2+}/Cu_2L^+	Cu_2L^+/Cu_2L	$Cu_2L^{2+} + H^+ /Cu_2LH^{2+}$	$Cu_2LH^{2+} + H^+/Cu_2LH_2^{2+}$	Cu_2LCl^+/Cu_2LCl	Cu_2LCl_2/Cu_2LCl_2
$E_0^{(1)} = +0.28$	$E_0^{(2)} = -0.91$	$HE_0^{(1)} = +0.03$	$HE_0^{(2)} = +0.21$	${}^{Cl}E_0^{(1)} = -0.88$	${}^{2Cl}E_0^{(1)} = -0.25$

tion). Nevertheless, we can extend the results of the previous section to AN solutions because when the water content is low the lack of protons surely favors route ***b***, that is, merging of the subsequent waves.

We can conclude that the effect of solvent observed in the system under study is in reality at least to a great extent the effect of protonation. The influence of solvent coordination to the reacting species as well as the effects of coordination with supporting anions in the bulk are comparatively minor as follows from our rough analysis of the kinetic parameters for various associated Cu_2L species. Hence, it is not possible to explain the acceleration of the Cu_2L reduction by chloride anions only in terms of an incompletely dissociating reactant. This is the reason why in the next section we address the "chloride catalysis" as the interfacial phenomenon.

(vi) Molecular Features of the Effect of Chloride Ions on the Cu_2L^{2+} Electroreduction. Two different scenarios of reduction of Cu_2L^{2+} species are suggested to explain the experimental results. The first one is the reduction of the adduct (Cu_2L^{2+} with chloride ions in the coordination sphere) formed in the solution bulk. We assumed a coexistence of two different complexes (Cu_2LCl^+ and Cu_2LCl_2) in electrolyte solutions with supporting Cl^- ions. DFT calculations were performed to obtain the equilibrium geometry of such complexes for oxidized and reduced states (see Figure 17). The Cu−Cl bond length values were calculated to be 0.238 nm (Cu_2LCl^+) and 0.243−246 nm (Cu_2LCl_2). The enthalpy values of the model reaction ($Cu_2L^{2+} + Cl^- = Cu_2LCl^+$) were calculated to be −1.13 eV (water) and −0.87 eV (AN), while a value of −2.52 eV (water) was obtained for the subsequent attachment of second chloride anion. The model redox potentials of their one-electron reduction steps are shown in Table 5. As can be seen from this table, the ${}^{Cl}E_0^{(1)}$ value is shifted significantly to negative potentials in comparison with $E_0^{(1)}$ (bare $[Cu_2L]^{2+}$ reduction) while the potential shift in the opposite direction is observed experimentally. Going to a neutral Cu_2LCl_2 complex a less negative value (${}^{2Cl}E_0^{(1)} = -0.25$ V) can be obtained (see Table 5) but the difference between $E_0^{(1)}$ and ${}^{2Cl}E_0^{(1)}$ still remains large.

The $\kappa_e$versus z dependency was calculated for the "planar" orientation of Cu_2LCl_2 (see Figure 13b). Using the PM3 method (see details in subsection (iii)), we examined additionally the distance of closest approach for Cu_2LCl_2 (0.6−0.7 nm reckoned from the electrode "edge"). As can be seen from Figure 13b, the electronic transmission coefficient exhibits no preferences for Cu_2LCl_2 compared to Cu_2L^{2+}. Moreover, the $\tilde{\lambda}_{in}$ values calculated for the reduction of Cu_2LCl^+ and Cu_2LCl_2 exceed those predicted earlier for Cu_2L^{2+} (see Table 3). This can be explained keeping in mind an additional reorganization of the Cu−Cl bonds. Thus, neither the FC barrier nor the pre-exponential factor point to Cu_2LCl^+ and Cu_2LCl_2 as the electrochemically active forms.

Electron transfer via an adsorbed Cl^- is regarded as the second mechanism. In this case the adsorbate facilitates ET because of the increased electronic transmission coefficient values (effect of the orbital overlap). The adsorption of Cl^- in three different surface sites (on-top, bridge, and hollow three-fold) was investigated on the basis of the cluster model. To obtain the equilibrium Cl−Hg distances, we performed additional DFT calculations. The uncharged mercury surface was modeled by a two-layer $Hg_{16}(10 + 6)$ cluster.[32] The valence electrons of mercury atoms were described by a basis set of DZ quality, while the inner shells were included in the Hay−Wadt effective core potential (ECP).[15] We employed the standard 6−311+g(d) basis set to describe the electrons of the Cl atom. No solvent effects were addressed for simplicity. Our calculations predict a small dependence of the adsorption energy on the surface corrugation: −2.50 eV (on-top and bridge sites) and −2.55 eV (hollow 3-fold site). Equilibrium Hg−Cl distances vary from 0.194 nm (hollow) to 0.28 nm (on-top). In further calculations the hollow position was assumed for Cl^-_{ads}. According to the Natural Population Analysis (NPA)[46] the charge of the adsorbed Cl^- ion (as well as calculated additionally Cl atom) is ≈ -0.9 e. The small partial charge transfer from the adsorbate to the metal may give some evidence in favor of the ≪ionic≫ nature of $Hg-Cl_{ads}$ bond.

If ET from Cl^-_{ads} is assumed, the electronic transmission coefficient can be estimated using eqs 6 and 7. In eq 8, which we employ to calculate the matrix element V_{if}, the $3p_z$ orbital of the Cl^-_{ads} (perpendicular to the metal surface) was taken as ψ_i and a small impurity from the wave functions of the

(46) Foster, J. P.; Weinhold, F. *J. Am. Chem. Soc.* **1980**, *102*, 7211–7218.

electrons in the Hg electrode was neglected. Bearing in mind the above mentioned results of the NPA analysis, one can suggest a value of ≈2 for the effective number of electrons contributing to ET (N_{eff}, see eq 7). The short Hg−Cl_{ads} bond should lead to a strong orbital overlap which provides, in turn, a very fast adiabatic ET from the mercury electrode to Cl_{ads} in the time scale of about 10^{-15} c (this process does not require an additional reorganization of the environment). Therefore, the mechanism we discuss differs from a frequently considered ≪bridge-assisted≫ ET[25,26] which needs a more complicated description. We have also examined different orientations of Cu_2L^{2+} relative to Cl^-_{ads}; the configuration portrayed in Figure 17b yields the highest k_e values.

The resulting data are plotted in Figure 14b. It is evident that the ≪adsorption≫ mechanism of ET leads to significantly larger κ_e values as compared with those obtained for the bare complex reactants. Note that the FC barrier in this case is the same as estimated for the Cu_2L^{2+} reduction while the redox potential should be shifted to more positive potentials because of the local interaction of Cu_2L^{2+} with Cl^-_{ads}. This may result in shorter distances of closest approach. Therefore, the second mechanism provides a more convincing explanation of the experimental data.

IV. Summary and Conclusions

Our experimental data exhibit the complex redox behavior of $[Cu_2L]Cl_2$ which is difficult to interpret in terms of a purely phenomenological approach. That is why we made an attempt to address the reaction mechanism at a molecular level. Emphasis was put on the estimations of the Franck−Condon barriers (contributions to the total reorganization energy) and the reactant-electrode orbital overlap effects (electronic transmission coefficients for different orientations) combining modern charge transfer theories and the results of DFT calculations. The Anderson Hamiltonian was employed to construct the FES describing the transfer of two electrons for different $[Cu_2L]Cl_2$ forms. Again, we have to stress a number of simplifications used in the model calculations. Although we cannot claim to a qualitative accuracy of our results, they are suitable to make qualitative predictions and provide a basis for the explanation of some trends observed in the experiment. The dual effect of protonation (both on the redox potential and on the reaction free energy surface) seems to be the most tempting for some extensions, as a considerable amount of the pertinent proton effects of similar sort can be found in the literature; see also a quantum chemical study of the electrochemical reactivity of deprotonated (hydrolyzed) In(III) aquacomplexes.[42c]

We studied the mercury surface−Cu_2L interaction to judge about the most probable distances of closest approach while the work terms were not properly addressed. More rigorous models, which might be employed in the future, presume the treatment of solvation effects in a more explicit way, for example, using QM/MM computational schemes. A more reliable estimation of the work terms also calls for considering the desorption of water molecules from the electrode surface. It would be also of worth to build a free energy surface describing the transfer of three or four electrons to gain more insight into the nature of the multistep reduction of $[Cu_2L]Cl_2$.

Besides the complex forms discussed above, we also explored some other possible adducts, $Cu_2L(CH_3CN)_2^{2+}$ and neutral $Cu_2L(CH_3COO)_2$ on the basis of DFT calculations. The intramolecular reorganization energies for both adducts were found to exceed that estimated for Cu_2L^{2+} (see Table 3). Because an effective size of the complexes is apparently larger as compared with Cu_2L^{2+}, the solvent reorganization is expected to be somewhat smaller. That is why at least comparable activation energy values may be predicted for all three complex forms (because of the mutual compensation of two different contributions to the total reorganization energy). Note, however, that the model k_e values estimated for the both adducts are noticeably smaller than those for Cu_2L^{2+} (mostly because of their larger size which entails larger distances of the closest approach for the most favorable "planar" orientation). These complex species can hardly be considered, therefore, as electrochemically active forms.

We believe that the approach proposed for analysis of multistep $[Cu_2L]Cl_2$ reduction might be of general interest for the electrochemistry of organic and coordination compounds with its typically complex reaction pathways. Futher steps presume quantitative prediction of reaction rates and should be supplemented by additional experimental efforts to determine partial rate constants by means of techniques that are beyond electrochemistry (like photoemission).[47]

Acknowledgment. We are indebted to Dr. Michael D. Bronshtein for useful comments. We are grateful as well to Prof. J. Heinze for the collaboration and the provided experimental setup. This work was supported in part by the RFBR (Project No. 05-03-32381a).

Supporting Information Available: This material is available free of charge via the Internet at http://pubs.acs.org.

IC702511W

(47) Krivenko, A. G., Kotkin, A. S., Simbirtseva, G. V., Nazmutdinov, R. R., Glukhov, D. V., Roznyatovskaya, N. V., Tsirlina, G. A., *Phys. Chem. Chem. Phys.* 2008, *10,* 2390 –2398.